IEEE Access
Multidisciplinary | Rapid Review | Open Access Journal

Date of publication xxxx 00, 0000, date of current version xxxx 00, 0000.

Digital Object Identifier 10.1109/ACCESS.2023.0322000

Plasma-Based Dual-Band Reflective Surface

MIRKO MAGAROTTO[1,2], (Member, IEEE), LUCA SCHENATO[1,2], (Member, IEEE), MARCO SANTAGIUSTINA[1,2], (Member, IEEE), ANDREA GALTAROSSA[1,2], (Fellow, IEEE), ANTONIO-D. CAPOBIANCO[1,2], (Member, IEEE)

[1]Department of Information Engineering, University of Padova, via Gradenigo 6/b, Padova, 35131, Italy (IT)
[2]National Inter-University Consortium for Telecommunications (CNIT), Viale Usberti 181/a, Parma, 43124, Italy (IT)

Corresponding author: Mirko Magarotto (e-mail: mirko.magarotto@unipd.it).

ABSTRACT The subject of this work is the numerical design of a plasma-based dual-band reflective surface. The proposed concept consists of a series of cylindrical plasma discharges placed on top of a reconfigurable surface made of conventional metallic patches. The possibility to independently control the steering of two signals, one in Ku-band (12.5 GHz) and the other in Ka-band (27.5 GHz), with a frequency ratio larger than 2, is proven. The signal at a lower frequency is controlled via the plasma density, while the one at a higher frequency is reconfigured via the conventional metallic surface. Notably, the larger the difference between the two working frequencies, the more a plasma-based reflecting surface suits dual-band operations.

INDEX TERMS Gaseous plasma antennas; Reflective surfaces; Dual-band; Ku-band; Ka-band.

I. INTRODUCTION

GASEOUS plasma antennas (GPAs) are devices in which the communication of electromagnetic (EM) signals relies on an ionized gas called plasma [1]. A notable property of GPAs is the capability to reconfigure their operation frequency [2] and radiation pattern [3], [4] by controlling the plasma density electronically. Moreover, when the antenna is not operating, the plasma is not energized and reverts to the neutral gas state [5]. Thus, a GPA can electrically disappear when plasma (i.e., the main conductive medium) fades [6]. Moreover, plasma is a dispersive medium whose EM response is frequency dependent [7]. This property can be exploited to integrate different GPAs into arrays or to realize broadband devices [8], [9]. A peculiar implementation of GPAs consists of reflective and transmissive surfaces [10], [11]. In these devices, plasma elements control EM waves' reflection [12] and/or transmission [13]. Some of the capabilities enabled by plasma-based surfaces are beam-steering [14], polarization control [15], and a combination of the two [16].

The rapid development of application fields such as 5G/6G communications [17]–[19] and satellite technology [20] has led to the adoption of high-frequency bands (e.g., Ka-band) to improve data transmission speed [21]. At the same time, lower frequency communications are still needed to satisfy specific requirements [22] or to exploit portions of the spectrum allocated for fixed services [23]. As a result, future scenarios will envision communication systems working at multiple frequencies alternatively or simultaneously [24]. This establishes the urgent need to develop dual-band devices that satisfy communication requirements while ensuring compactness and minimizing costs [17]. Shared-aperture phased antenna arrays have been proposed to control the radiation pattern in Ku- and Ka-bands [20], [25]. In these devices, elements operating in different frequency bands are integrated into a common aperture [26], both staggered or overlapped on different layers [27]. Shared-aperture antennas can achieve a very large frequency ratio, which is required, for example, in the field of 5G/6G to integrate communications in S- and Ka-bands [17], [28] or S- and V-bands [29]. A peculiar implementation of shared-aperture technology envisions housing both a low-frequency patch array and a high-frequency reflectarray in the same aperture area to achieve dual-band operations in S- and Ka-bands, respectively [30]. Nonetheless, shared-aperture antennas require complex systems to control the signal phase at each array port, so alternative solutions are proposed in the literature to exploit dual-band [31]. Reflectarrays are a particularly consolidated technology in satellite communications to handle signals in Ku- and Ka-bands [32], [33]. Nonetheless, the most mature solutions involving several resonant elements organized in multiple layers are not reconfigurable [34]. In

reflectarrays, reconfigurability comes at the cost of a reduced frequency ratio (e.g., two frequencies embedded in the Ku-band) [35]. Some examples include 1-bit reflectarrays operated in X- and Ku-bands, which integrate phase-shifters [36] or PIN-diodes [37]. To the authors' knowledge, the only solution proposed to realize a reflectarray with a frequency ratio larger than 2 (i.e., operations in X- and Ka-bands) envisions a unit cell based on the barium-strontium-titanate technology [38]. Nonetheless, this solution causes relatively high reflection losses ($>$ 10 dB), and tests described in the literature concern only a single unit cell, not the overall array. Another technology proposed to implement dual-band operations is metasurfaces in which the unit cells consist of sub-wavelength resonators [39]. Nevertheless, also with this solution, reconfigurability comes at the cost of a relatively reduced frequency ratio (e.g., X- and Ku-band) [40]–[42]. Even though examples of metasurfaces handling signals in Ka- and V-bands are available in the literature [43], they need to be integrated into arrays of dual-band antennas, increasing the complexity of the overall system. Finally, transmittarrays have been proposed to handle Ku- and Ka-bands simultaneously [44] or K- and Ka-bands [45]. To sum up, the solutions that combine reconfigurability and large frequency ratio, say > 2, are not optimal because of their complexity. Therefore, there is the need to identify alternatives to enable these properties in reflectarrays and/or metasurfaces.

The scope of this work is to present the numerical design of the first reflecting surface, operating in the tens of GHz range, that is reconfigurable and enables a frequency ratio larger than 2. The proposed solution consists of a plasma-based dual-band reflective surface. Notably, the proposed device is also the first GPA that allows a frequency ratio > 2. In fact, even though GPAs are proven to enable multi-frequency [2] and broadband [9] operations, this is limited to hundreds of MHz given a central frequency in the order of $1-2$ GHz. In the following, the lower frequency signal is in the Ku-band (12.5 GHz), and the higher frequency one is in the Ka-band (27.5 GHz). In particular, these two frequencies are adopted for the downlink and uplink signals in satellite communications [46]. Last but not least, a plasma-based system does not rely on resonating elements [14]. So, the two working frequencies can be easily tuned considering that, as proven later, the larger the spam between them, the better the proposed surface is suitable for dual-band operations.

II. METHODOLOGY

Plasma is treated as a dispersive medium whose relative permittivity ε_p is computed via the Drude model [14], [47]:

$$\varepsilon_p = 1 - \frac{\omega_p^2}{\omega^2+\nu^2} + j\frac{\nu}{\omega}\frac{\omega_p^2}{\omega^2+\nu^2}\,, \tag{1}$$

where ω_p is the plasma frequency in rad/s, ν is the collision frequency in Hz, and ω is the wave frequency in rad/s. The plasma frequency reads

$$\omega_p = \sqrt{\frac{q^2 n_e}{m\varepsilon_0}}\,, \tag{2}$$

where q is the elementary charge, m the electron mass, ε_0 the vacuum permittivity, and n_e the plasma density. Thus, the EM response of the plasma can be controlled by varying electronically n_e and, in turn, ω_p [48]. The collision frequency reads

$$\nu = n_0 K(T_e)\,, \tag{3}$$

where n_0 is the neutral gas density, and K is a rate constant that depends on the gas type and the electron temperature T_e. In this work, argon gas is considered [49]. In particular, ν is associated with Ohmic losses and is proportional to the amount of residual neutral gas [50]. It is worth defining the critical density

$$n_e^{cr} = m\varepsilon_0\left(\frac{2\pi f}{q}\right)^2\,, \tag{4}$$

where $f = \omega/2\pi$ is the wave frequency in Hz. Given that in usual GPAs $\nu \ll \omega_p$ [51], $\mathrm{Re}(\varepsilon_p) > 0$ if $n_e < n_e^{cr}$. Namely, waves can propagate in plasma if $n_e < n_e^{cr}$, else they are evanescent [12].

Numerical simulations are performed with the commercial software CST Studio Suite ®. The computational domain has been discretized on an unstructured tetrahedral mesh, and Maxwell's equations are integrated in the frequency domain. Plasma is handled relying on the native dispersion model called "Drude" which implements ε_p as prescribed in Eq. 1. A plane wave is assumed to impinge the structure at hand propagating along the z-direction of a Cartesian reference frame. The wave is linearly polarized along the y-direction. Three different kinds of analysis have been performed: concept analysis (see section III), Floquet analysis (see section IV), and array analysis (see section V). In the first and second cases, unit cells are studied adopting Floquet boundary conditions on the x- and y-directions while open conditions are assumed along the z-direction [52]. Because of these settings, the unit cells are considered as the constitutive elements of an infinite periodic structure extending along the x- and y-directions. The performance is evaluated in terms of the scattering parameters S_{11} and S_{21}

$$S_{11} = \frac{E_\rho}{E_\iota}\,, \tag{5a}$$

$$S_{21} = \frac{E_\tau}{E_\iota}\,, \tag{5b}$$

where E_ι, E_ρ, E_τ are complex versors associated with the incident, reflected and transmitted electric field, respectively [52]. Namely, S_{11} describes the reflected wave while S_{21} the transmitted one. On the other hand, the array analysis aims to assess the capability of a plasma-based reflective surface to perform beam steering in dual-band operation. To this end, a finite-size reflective surface, not an infinitely periodized unit cell, is simulated by imposing open conditions along all directions. In this case, the performance is evaluated via the radar cross section (RCS) [53].

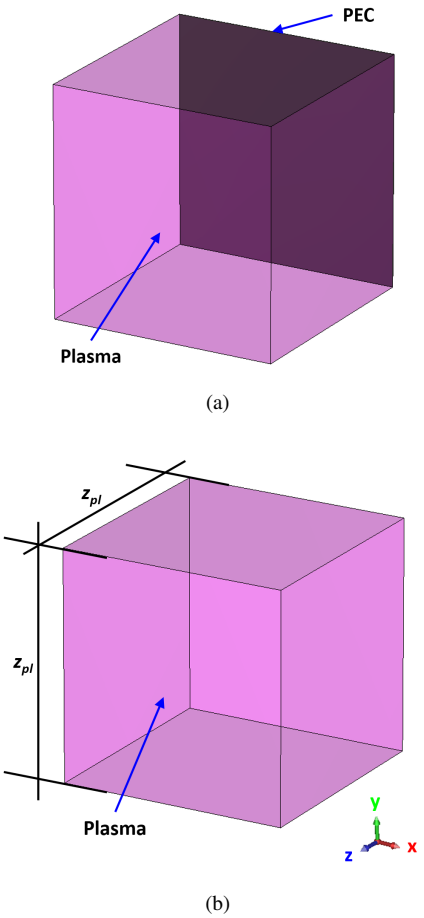

FIGURE 1. Unit cells handled in the concept analysis: (a) reflection and (b) transmission mode.

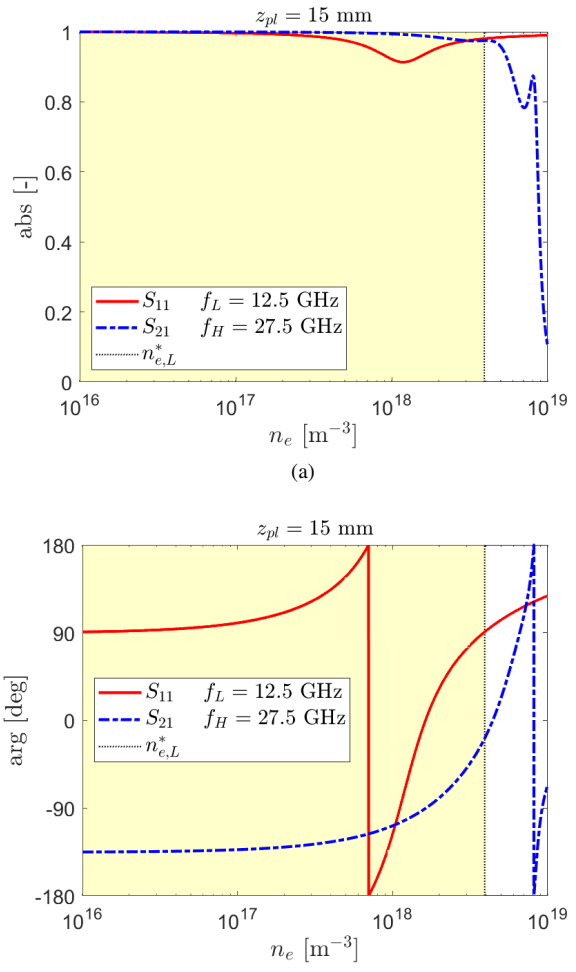

FIGURE 2. (a) Amplitude and (b) phase of S_{11} at f_L, and S_{21} at f_H in function of the plasma density n_e. The threshold value to reconfigure the phase of S_{11} over 360° is $n^*_{e,L}$.

III. CONCEPT ANALYSIS

The feasibility of a plasma-based dual-band reflective surface is preliminary assessed via the simplified unit cells depicted in Fig. 1. A uniform plasma cube of side $z_{pl} = 15$ mm is analysed in reflection mode at $f_L = 12.5$ GHz (see Fig. 1a) and in transmission mode at $f_H = 27.5$ GHz (see Fig. 1b). The plasma cube is assumed to be placed on top of a perfect electric conductor (PEC) plate in reflection mode, while this component is not present in transmission mode. Thus, $S_{21} = 0$ in the former case. The Floquet boundary conditions applied to the unit cells depicted in Fig. 1 result in a plasma slab with an infinite extension along the x- and y-directions [12]. Notably, $z_{pl} \approx 0.6\lambda_L$, where λ_L is the wavelength in vacuum associated with the signal at frequency f_L. A realistic value for the collision frequency is assumed $\nu = 1.57$ GHz [54].

The scattering parameters S_{11} and S_{21}, computed in reflection and transmission mode, respectively, are depicted in Fig. 2. Consistently with previous theoretical analyses [12], it is possible to control the phase of the reflected signal at f_L over 360° varying the plasma density in the interval $n_e \leq n^*_{e,L}$. In this range, $|S_{11}| > 0.9$, so mild Ohmic losses affect wave propagation in plasma. More interestingly, $|S_{21}| > 0.9$ in the interval $n_e \leq n^*_{e,L}$, which means that the plasma is almost transparent with respect to the signal at f_H. This result confirms the possibility of realizing a plasma-based dual-band reflective surface. In fact, plasma can be employed to control the reflection of the signal at f_L while an additional substrate shall be included in the ground plane to handle the signal at f_H, which can propagate through the plasma. In this case, $\arg(S_{21})$ is affected by the propagation through the plasma slab (see Fig. 2b). Thus, the substrate that controls the signal at f_H shall compensate for this predictable phase shift.

In general, $|S_{21}| \approx 1$ for $n_e \lesssim n^{cr}_e$ since, in this interval, waves can propagate in plasma [55]. Therefore, a necessary condition for the feasibility of a plasma-based dual-band reflective surface is

$$n^*_{e,L} \lesssim n^{cr}_{e,H}\,, \tag{6}$$

where $n^*_{e,L}$ is the threshold density to reconfigure the signal at f_L in a certain phase range [56] and $n^{cr}_{e,H}$ identifies the

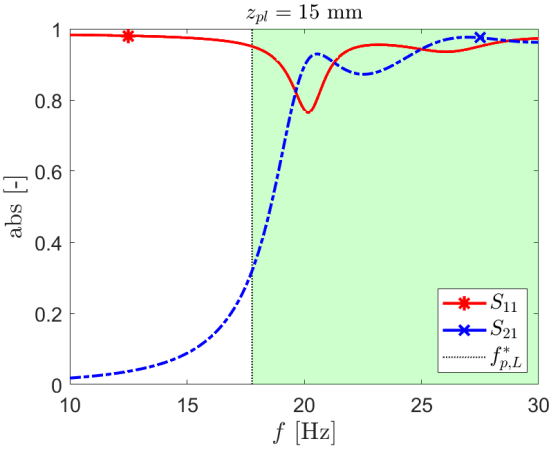

FIGURE 3. Amplitude of the scattering parameters S_{11} and S_{21} vs. wave frequency f for $n_e = n^*_{e,L}$. Markers correspond to f_L and f_H, respectively. The plasma frequency $f^*_{p,L}$ sets a lower bound for f_H.

upper limit to maintain $|S_{21}| \approx 1$ for the signal at f_H. It is practical to reformulate Eq. 6 as follows

$$f_H \gtrsim f^*_{p,L}\,, \tag{7}$$

where $f^*_{p,L}$ is the plasma frequency, in Hz, for $n_e = n^*_{e,L}$. In fact, Eq. 7 can be interpreted through Fig. 3, where the amplitude of S_{11} and S_{21} is depicted in function of the wave frequency.In the case at hand, the condition $f_H \geq 20$ GHz shall be enforced to guarantee $|S_{21}| \approx 1$. To sum up, the larger the difference between f_L and f_H, the more a plasma-based reflecting surface is suitable for dual-band operations.

IV. FLOQUET ANALYSIS

The realistic design of a plasma-based dual-band reflective surface is discussed, beginning with analyzing its constitutive unit cells (see Fig. 4). A design procedure is proposed starting from the separate analysis of a "plasma" unit cell aimed at controlling the signal at $f_L = 12.5$ GHz (see Fig. 4a) and a "patch" unit cell dedicated to the signal at $f_H = 27.5$ GHz (see Fig. 4b). These results are merged to define the "combined" unit cell that constitutes the plasma-based dual-band reflective surface (see Fig. 4c). Specifically, the plasma unit cell consists of two cylindrical plasma discharges placed on top of a PEC ground plane consistently with the realistic design proposed in [47]. The patch unit cell is constituted by metallic squares connected via varactors and placed on top of a dielectric layer and a PEC ground plane. This is consistent with the solution proposed in [57] and represents a generic substrate designed to handle the signal at f_H [58].

The periodicity of the considered unit cells is $p = 0.5\lambda_H = 0.23\lambda_L = 5.5$ mm where λ_H is the wavelength in vacuum for the signal at f_H. Namely, this value is selected to avoid the presence of grating lobes at both operation frequencies [59]. Given that the size and periodicity of the unit cells are in the order of some parts of the wavelength, this structure cannot be rigorously addressed as a metasurface [60]. Consequently, the resultant plasma-based reflective

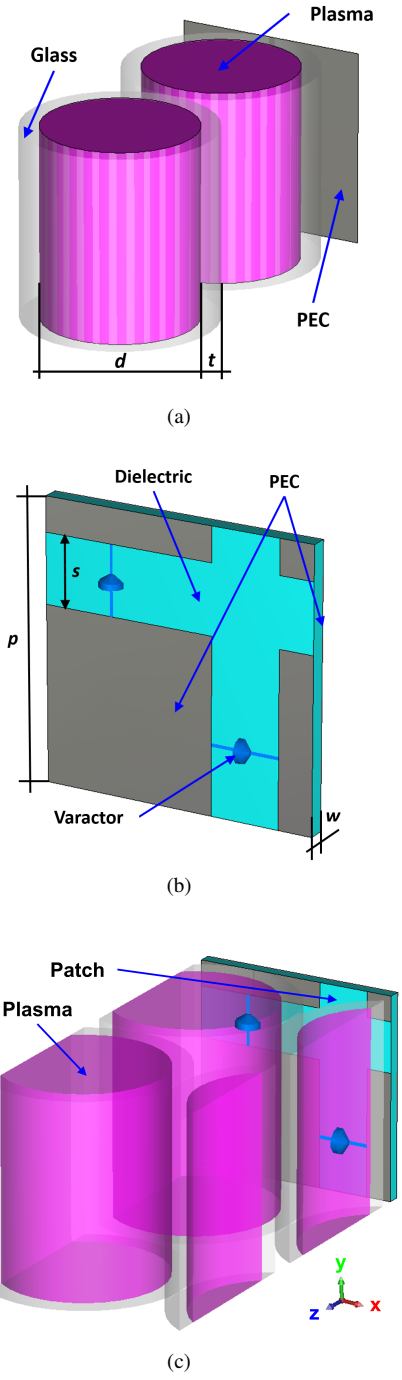

FIGURE 4. Unit cells handled in the Floquet analysis: (a) plasma, (b) patch, and (c) combined.

surface has been treated as a reflectarray, and modeled accordingly, given that the local surface homogenization should not be applied [60]. The elements that constitute the plasma unit cell are cylinders of height and diameter p, where the plasma columns have diameter $d = 0.8p = 4.5$ mm and are encased in a glass vessel of thickness $t = 0.1p = 0.5$ mm, relative permittivity $\varepsilon_g = 4.82$ and loss tangent $\tan\delta_g = 5.4 \times 10^{-3}$. For the plasma medium, the collision

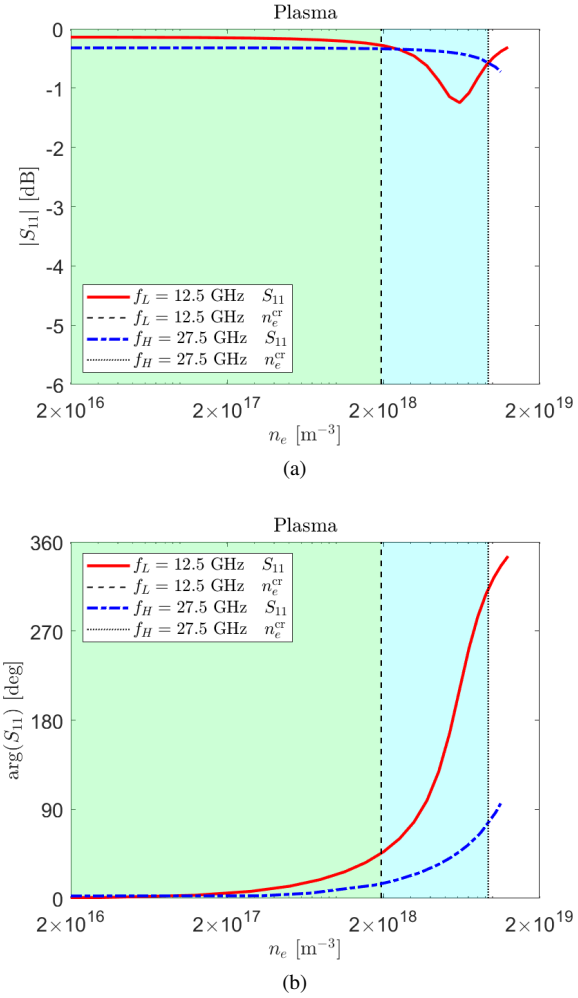

FIGURE 5. Plasma unit cell: (a) amplitude and (b) phase of the scattering parameter S_{11} as a function of the plasma density n_e. Comparison between results at f_L and f_H. The colored background indicates the intervals in which waves propagate within the plasma.

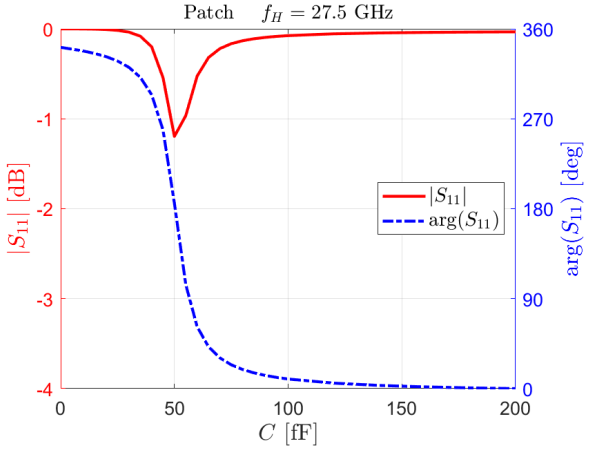

FIGURE 6. Patch unit cell: amplitude and phase of the scattering parameter S_{11} vs. varactor capacitance C.

frequency is $\nu = 1.57$ GHz [54]. The patch unit cells rely on a dielectric layer of thickness $w = 0.06p = 0.3$ mm and relative permittivity $\varepsilon_d = 2.2$ (i.e., Rogers RT/duroid 5880). Metallic squares are separated from one another by a distance $s = 0.25p = 1.4$ mm; namely, their side is equal to $D = 0.75p = 4.1$ mm. Varactors are simulated as an RC series circuit where the resistance is $R = 1\ \Omega$, and the capacitance C is variable [57].

A. PLASMA

The parameter S_{11} for the plasma unit cell (see Fig. 4a) is reported in Fig. 5. Both the signals at f_L and f_H have been analyzed. Maintaining $n_e \lesssim 10^{19}$ m^{-3}, it is possible to reconfigure the phase of the signal at f_L of about 340° ensuring $|S_{11}| > -1.2$ dB. At the same time, $n_e^{cr} \approx 10^{19}$ m^{-3} for the signal at f_H, so the proposed unit cell falls within the limit prescribed by Eq. 6 for the feasibility of a plasma-based dual-band reflective surface. Due to the interaction with the plasma medium, the signal at f_H is subject to mild Ohmic losses and a maximum phase shift of 90° that the patch substrate shall compensate. The values of $\arg(S_{11})$ are normalized in order to equal 0° when $n_e \to 0$.

Other plasma unit cell designs can take a larger margin with respect to the condition established by Eq. 6. For example, adding a third plasma discharge would allow reconfiguring $\arg(S_{11})$ over 360° maintaining $n_{e,L}^* < 10^{19}$ m^{-3} [12], [14], [47], namely farther away from $n_{e,H}^{cr}$. But, this solution would increase the technological complexity of the design.

B. PATCH

For the patch unit cell (see Fig. 4b), the parameter S_{11} referred to the signal at f_H is reported in Fig. 6. Keeping $C < 200$ fF, it is possible to reconfigure the phase of the scattering parameter over 340° maintaining $|S_{11}| > -1.2$ dB. The value of $\arg(S_{11})$ is normalized to equal 0° when $C = 200$ fF. Even for the patch unit cell, other designs are available if $\arg(S_{11})$ shall be controlled over 360° [61]. Nonetheless, a higher complexity level is required to implement these solutions (e.g., multi-layer patches), and, as proven in section IV-C, they are not needed for the case at hand. Moreover, it is worth mentioning that the patch substrate behaves almost as a ground plane for the signal at f_L. Namely, the values of C adopted in the present design (see Table 1) cause a variation of $\arg(S_{11})$ in the range of some degrees.

C. COMBINED

Once the behavior of the plasma and patch unit cells is known, a procedure is needed to select the values of n_e and C to control the EM waves' reflection. If the value of C does not have a major impact on the signal at f_L, the parameter n_e can be selected from Fig. 5, say via the array factor rule [53], to induce a certain steering angle $\theta_L^{\max}$. Provided these values of n_e, C can be selected to impose a second steering angle $\theta_H^{\max}$ to the signal at f_H compensating the phase shift due to the plasma. As proven in Fig. 7, the latter procedure can be

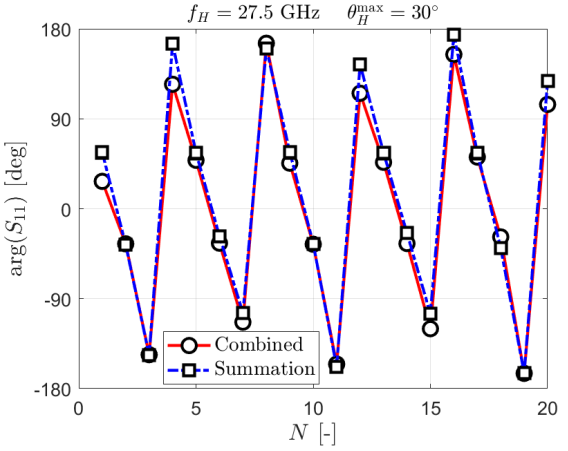

FIGURE 7. Combined unit cell: phase of the reflection coefficient Γ_0 vs. column number N to get $\theta_H^{\max} = 30°$. The results obtained according to Table 1 ("Combined") are compared against the superposition of the effects given by plasma and patch unit cells ("Summation").

TABLE 1. Plasma density (n_e [10^{18} m^{-3}]) and capacitance (C [fF]) sorted by column (N [-]) to obtain $\theta_H^{\max} = 30°$ and $\theta_L^{\max} = -30°$.

N	1	2	3	4	5	6	7	8	9	10
n_e	0	1.7	3.3	4.4	5.3	6.0	6.9	8.1	10.5	0.3
C	65	39	49	56	168	44	51	59	34	36
N	11	12	13	14	15	16	17	18	19	20
n_e	2.1	3.5	4.6	5.4	6.2	7.1	8.4	11.3	0.7	2.4
C	49	55	114	44	51	58	16	48	48	54

accomplished via the superposition of the effects

$$\arg(S_{11}) \approx \arg(S_{11}^{\text{plasma}}) + \arg(S_{11}^{\text{patch}}) - 180° \,. \quad (8)$$

Namely, the phase of the scattering parameter computed with the combined unit cell $\arg(S_{11})$ is almost equal to the plasma contribution $\arg(S_{11}^{\text{plasma}})$ plus the patch contribution $\arg(S_{11}^{\text{patch}})$. The 180° term is needed to correctly account for the reflection occurring at the ground plane. Clearly, the terms $\arg(S_{11}^{\text{plasma}})$ and $\arg(S_{11}^{\text{patch}})$ in Eq. 8 refer to the signal at f_H and are depicted in Fig. 5 and Fig. 6, respectively.

The results in Fig. 7 are obtained assuming the values of n_e and C reported in Table 1. The latter is obtained via the proposed design strategy imposing $\theta_H^{\max} = 30°$ and $\theta_L^{\max} = -30°$. In particular, a structure of 20 uniform columns that induce steering in the azimuth plane (x-z) has been considered. Notably, the computations performed with the combined unit cell ("Combined") and the superposition of the effects ("Summation") fairly match.

It is worth mentioning that if the variation of C has a significant effect on the signal at f_L, the design of the combined unit cell is not straightforward, given that n_e and C shall be selected simultaneously to satisfy the requirements imposed

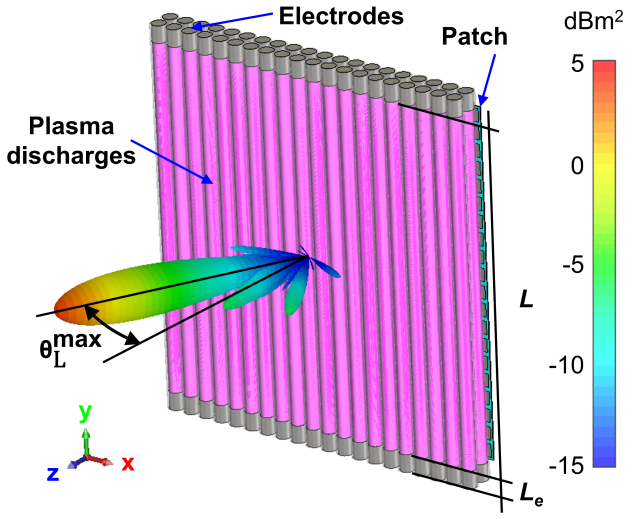

FIGURE 8. Reflective surface handled in the array analysis. The structure consists of 20 pairs of plasma discharges placed on top of a substrate composed of 20×20 patch elements. Radar cross section (RCS) evaluated at f_L according to the data reported in Table 1.

at both operation frequencies. Nonetheless, this does not prevent the possibility of realizing a plasma-based dual-band reflective surface. At the same time, the assumption of the array factor rule to implement wave deflection is not always optimal when applied to a reflective surface [62]. For example, based on a proper surface local impedance definition, advanced syntheses techniques are available to handle reflective surfaces, implemented via metasurfaces [62].

V. ARRAY ANALYSIS

The unit cell proposed in section IV has been exploited to numerically design a plasma-based dual-band reflective surface (see Fig. 8). The structure comprises 20 pairs of plasma discharges [47] placed on top of a substrate realized with 20×20 patch elements. Columns are enumerated (N) from negative to positive values of the x-axis. The plasma tubes, encased in a glass vessel, are long $L = 20p = 109$ mm and terminate in metal electrodes of length p and diameter d. All the other dimensions are consistent with the values reported in section IV. As pointed out in [47], this configuration enables the control of the signal at f_L only in the azimuth plane (x-z). To implement reconfigurability also in elevation, square plasma elements would be needed [12]. Nonetheless, cylindrical plasma discharges are a technology at the state of the art [6], so they have been preferred with respect to more exotic implementations.

The radiation pattern depicted in Fig. 8 refers to the signal at f_L and has been obtained assuming the values of n_e and C reported in Table 1. In particular, Fig. 9 shows the RCS in the azimuth plane for two different configurations of the plasma-based reflective surface. The steering angle of the higher frequency signal is $\theta_H^{\max} = 30°$ and $\theta_H^{\max} = -30°$, respectively, while the main lobe at lower frequency is main-

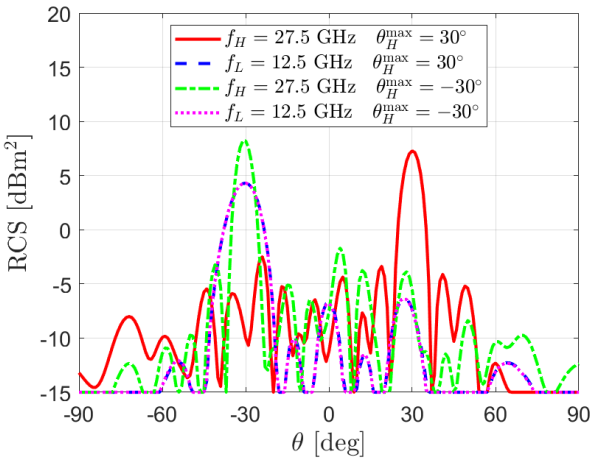

FIGURE 9. Radar cross section (RCS) vs azimuth angle θ evaluated at f_L and f_H, imposing a fixed $\theta_L^{\max} = -30°$ and for two different values of $\theta_H^{\max} = 30°$ (see Table 1), and $\theta_H^{\max} = -30°$ (see Table 2).

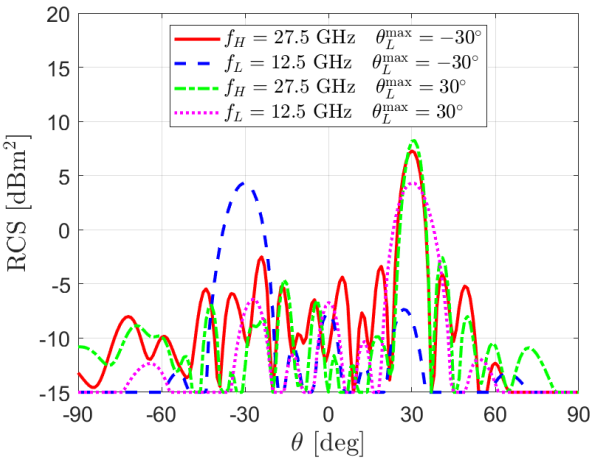

FIGURE 10. Radar cross section (RCS) vs azimuth angle θ evaluated at f_L and f_H, imposing a fixed $\theta_H^{\max} = 30°$ and for two different values of $\theta_L^{\max} = -30°$ (see Table 1), and $\theta_L^{\max} = 30°$ (see Table 3).

TABLE 2. Plasma density (n_e [10^{18} m^{-3}]) and capacitance (C [fF]) sorted by column (N [-]) to obtain $\theta_H^{\max} = -30°$ and $\theta_L^{\max} = -30°$.

N	1	2	3	4	5	6	7	8	9	10
n_e	0	1.7	3.3	4.4	5.3	6.0	6.9	8.1	10.5	0.3
C	65	54	49	43	168	57	51	46	34	53
N	11	12	13	14	15	16	17	18	19	20
n_e	2.1	3.5	4.6	5.4	6.2	7.1	8.4	11.3	0.7	2.4
C	49	42	114	56	51	45	16	68	48	40

TABLE 3. Plasma density (n_e [10^{18} m^{-3}]) and capacitance (C [fF]) sorted by column (N [-]) to obtain $\theta_H^{\max} = 30°$ and $\theta_L^{\max} = 30°$.

N	1	2	3	4	5	6	7	8	9	10
n_e	2.4	0.7	11.3	8.4	7.1	6.2	5.4	4.6	3.5	2.1
C	40	48	68	16	45	51	56	114	42	49
N	11	12	13	14	15	16	17	18	19	20
n_e	0.3	10.5	8.1	6.9	6.0	5.3	4.4	3.3	1.7	0
C	53	34	46	51	57	168	43	49	54	65

tained at $\theta_L^{\max} = -30°$. The reflected beam is reconfigured in this way by keeping the same n_e values and by tuning C as prescribed in Table 1 and Table 2, respectively. The two configurations perfectly satisfy the design requirements ensuring a side lobe level SLL ≈ -10 dB. Spurious lobes at both frequencies are due to the finite-size of the proposed reflective surface as well as the adoption of the array factor rule to design the structure [62]. Differences lower than 0.1 dB are notably registered between the two signals at f_L. Thus, the reflected wave at f_H can be controlled by acting only on the conventional metallic patches via the C values without any major effect on the signal at f_L, which is controlled by the plasma elements through the n_e values.

On the contrary, Fig. 10 shows the RCS for the other two configurations, which vary the direction of the reflected beam at lower frequency ($\theta_L^{\max} = \pm 30°$) while keeping the one at higher frequency fixed ($\theta_H^{\max} = 30°$). In this case, both n_e and C shall be controlled since, even though the signal at f_H is driven by the C values, changing n_e to reconfigure the signal at f_L causes a variation of the phase shift to be compensated. This is not a major issue given that the phase shift induced by the plasma is predictable as it is the corresponding value of C needed to compensate for it. Notably, the proposed design satisfies the imposed requirements ensuring SLL ≈ -10 dB.

VI. CONCLUSIONS

The numerical design of a plasma-based dual-band reflective surface has been presented. The proposed concept operates in the Ku- and Ka-bands being the first GPA ensuring a frequency ratio larger than 2. A plasma-based reflective surface is better for handling dual-band operations if the difference between the two working frequencies is large (i.e., in the tens of GHz range). In fact, the signal at a lower frequency depends on the plasma density, while the one at a higher frequency can be controlled via varactors integrated into a dedicated patch substrate. A simplified design procedure is proposed if the signal at a lower frequency is mildly affected by the varactors' parameters.

The realization and test of the proposed concept will be the subject of future work. Indeed, a plasma-based dual-band reflective surface is challenging. First, the electronics to sustain the plasma shall be improved in terms of miniaturization and stability in time. This task has been solved in the frame

of space electric propulsion [63], [64], but effort is required to apply such improvements in the field of plasma-based reflective surfaces. Second, metasurfaces that operate in Ka-band are available in the literature [58] but their realization and test are non-trivial. Thus effort is required to integrate a suitable patch substrate in a plasma-based reflective surface. Nonetheless, the plasma properties assumed in this work are realistic, and the simulated plasma discharges are compatible with the technology at the state of the art [6], [54]. Thus, plasma-based dual-band reflective surfaces are demanding but feasible.

ACKNOWLEDGMENT

This work was partially supported by the European Union under the Italian National Recovery and Resilience Plan (NRRP) of NextGenerationEU, partnership on "Telecommunications of the Future" (PE00000001 - program "RESTART"). Authors thank Dr. Paola De Carlo for the insightful conversations on the main subject of this work.

REFERENCES

[1] T. Anderson, *Plasma antennas*. Artech House, 2020.

[2] F. Sadeghikia, M. R. Dorbin, A. K. Horestani, M. T. Noghani, and H. Ja'afar, "Tunable inverted-f antenna using plasma technologies," *IEEE Antennas and Wireless Propagation Letters*, vol. 18, no. 4, pp. 702–706, 2019.

[3] C. Wang, W. Shi, B. Yuan, and J. Mao, "Pattern-steerable endfire plasma array antenna," *IEEE Transactions on Antennas and Propagation*, vol. 69, no. 10, pp. 6994–6998, 2021.

[4] G. Mansutti *et al.*, "Design of a hybrid metal-plasma transmit-array with beam-scanning capabilities," *IEEE Transactions on Plasma Science*, vol. 50, no. 3, pp. 662–669, 2022.

[5] M. Magarotto *et al.*, "Numerical suite for gaseous plasma antennas simulation," *IEEE Transactions on Plasma Science*, vol. 49, no. 1, pp. 285–297, 2020.

[6] P. De Carlo *et al.*, "Experimental characterization of a plasma dipole in the uhf band," *IEEE Antennas and Wireless Propagation Letters*, vol. 20, no. 9, pp. 1621–1625, 2021.

[7] T. Naito, S. Yamaura, Y. Fukuma, and O. Sakai, "Radiation characteristics of input power from surface wave sustained plasma antenna," *Physics of Plasmas*, vol. 23, no. 9, p. 093504, 2016.

[8] H. A. E.-A. Malhat and A. S. Zainud-Deen, "Dual/circular polarization beam shaping of time-modulated plasma-based magneto-electric dipole antenna arrays," *Optical and Quantum Electronics*, vol. 54, no. 2, p. 111, 2022.

[9] C. Wang, B. Yuan, W. Shi, and J. Mao, "Low-profile broadband plasma antenna for naval communications in vhf and uhf bands," *IEEE Transactions on Antennas and Propagation*, vol. 68, no. 6, pp. 4271–4282, 2020.

[10] M. Magarotto, L. Schenato, M. Santagiustina, A. Galtarossa, and A.-D. Capobianco, "Plasma-based reflecting and transmitting surfaces," *IEEE Access*, vol. 11, pp. 91 196–91 205, 2023.

[11] H. A. E.-A. Malhat, M. M. Badawy, S. H. Zainud-Deen, and K. H. Awadalla, "Dual-mode plasma reflectarray/transmitarray antennas," *IEEE Transactions on Plasma Science*, vol. 43, no. 10, pp. 3582–3589, 2015.

[12] M. Magarotto, L. Schenato, P. De Carlo, and A.-D. Capobianco, "Feasibility of a plasma-based intelligent reflective surface," *IEEE Access*, vol. 10, pp. 97 995–98 003, 2022.

[13] S. H. Zainud-Deen, H. A. E.-A. Malhat, S. M. Gaber, and K. H. Awadalla, "Beam steering plasma reflectarray/transmitarray antennas," *Plasmonics*, vol. 9, pp. 477–483, 2014.

[14] M. Magarotto *et al.*, "Feasibility study on a plasma based reflective surface for satcom systems," *Acta Astronautica*, vol. 208, pp. 55–61, 2023.

[15] M. Magarotto, L. Schenato, P. De Carlo, and A.-D. Capobianco, "Plasma-based reflective surface for polarization conversion," *IEEE Transactions on Antennas and Propagation*, vol. 71, no. 3, pp. 2849–2854, 2023.

[16] M. Magarotto, L. Schenato, M. Santagiustina, A. Galtarossa, and A.-D. Capobianco, "Plasma-based intelligent reflecting surface for beam-steering and polarisation conversion," *IEEE Access*, vol. 11, pp. 43 546–43 556, 2023.

[17] F. Xiao, X. Lin, and Y. Su, "Dual-band structure-shared antenna with large frequency ratio for 5G communication applications," *IEEE Antennas and Wireless Propagation Letters*, vol. 19, no. 12, pp. 2339–2343, 2020.

[18] M. Giordani, M. Polese, M. Mezzavilla, S. Rangan, and M. Zorzi, "Toward 6g networks: Use cases and technologies," *IEEE Communications Magazine*, vol. 58, no. 3, pp. 55–61, 2020.

[19] E. Basar, M. Di Renzo, J. De Rosny, M. Debbah, M.-S. Alouini, and R. Zhang, "Wireless communications through reconfigurable intelligent surfaces," *IEEE access*, vol. 7, pp. 116 753–116 773, 2019.

[20] Y. R. Ding and Y. J. Cheng, "Ku/Ka dual-band dual-polarized shared-aperture beam-scanning antenna array with high isolation," *IEEE Transactions on Antennas and Propagation*, vol. 67, no. 4, pp. 2413–2422, 2019.

[21] X. Liu, K.-Y. Lam, F. Li, J. Zhao, L. Wang, and T. S. Durrani, "Spectrum sharing for 6G integrated satellite-terrestrial communication networks based on NOMA and CR," *IEEE Network*, vol. 35, no. 4, pp. 28–34, 2021.

[22] B. J. Xiang, S. Y. Zheng, H. Wong, Y. M. Pan, K. X. Wang, and M. H. Xia, "A flexible dual-band antenna with large frequency ratio and different radiation properties over the two bands," *IEEE Transactions on Antennas and Propagation*, vol. 66, no. 2, pp. 657–667, 2017.

[23] E. Martinez-de Rioja, J. A. Encinar, M. Barba, R. Florencio, R. R. Boix, and V. Losada, "Dual polarized reflectarray transmit antenna for operation in Ku- and Ka-bands with independent feeds," *IEEE Transactions on Antennas and Propagation*, vol. 65, no. 6, pp. 3241–3246, 2017.

[24] D. Minoli and B. Occhiogrosso, "Practical aspects for the integration of 5G networks and iot applications in smart cities environments," *Wireless Communications and Mobile Computing*, vol. 2019, 2019.

[25] S. Liu, K. Jiang, G. Xu, X. Ding, K. Zhang, J. Fu, and Q. Wu, "A dual-band shared aperture antenna array in Ku/Ka-bands for beam scanning applications," *IEEE Access*, vol. 7, pp. 78 794–78 802, 2019.

[26] D. M. Pozar and S. D. Targonski, "A shared-aperture dual-band dual-polarized microstrip array," *IEEE Transactions on Antennas and Propagation*, vol. 49, no. 2, pp. 150–157, 2001.

[27] J. Ran, Y. Wu, C. Jin, P. Zhang, and W. Wang, "Dual-band multi-polarized aperture-shared antenna array for Ku-/Ka-band satellite communication," *IEEE Transactions on Antennas and Propagation*, 2023.

[28] T. Li and Z. N. Chen, "Shared-surface dual-band antenna for 5G applications," *IEEE Transactions on Antennas and Propagation*, vol. 68, no. 2, pp. 1128–1133, 2019.

[29] J. F. Zhang, Y. J. Cheng, Y. R. Ding, and C. X. Bai, "A dual-band shared-aperture antenna with large frequency ratio, high aperture reuse efficiency, and high channel isolation," *IEEE Transactions on Antennas and Propagation*, vol. 67, no. 2, pp. 853–860, 2018.

[30] D. E. Serup, G. F. Pedersen, and S. Zhang, "Dual-band shared aperture reflectarray and patch antenna array for S- and Ka-bands," *IEEE Transactions on Antennas and Propagation*, vol. 70, no. 3, pp. 2340–2345, 2021.

[31] N. J. Fonseca and C. Mangenot, "High-performance electrically thin dual-band polarizing reflective surface for broadband satellite applications," *IEEE Transactions on Antennas and Propagation*, vol. 64, no. 2, pp. 640–649, 2015.

[32] P. Naseri, M. Riel, Y. Demers, and S. V. Hum, "A dual-band dual-circularly polarized reflectarray for K/Ka-band space applications," *IEEE Transactions on Antennas and Propagation*, vol. 68, no. 6, pp. 4627–4637, 2020.

[33] J. Zhao, T. Li, X. Cui, X. Zhao, H. Li, B. Hu, H. Wang, Y. Zhou, and Q. Liu, "A low-mutual coupling dual-band dual-reflectarray antenna with the potentiality of arbitrary polarizations," *IEEE Antennas and Wireless Propagation Letters*, vol. 16, pp. 3224–3227, 2017.

[34] D. Martinez-de Rioja, R. Florencio, E. Martinez-de Rioja, M. Arrebola, J. A. Encinar, and R. R. Boix, "Dual-band reflectarray to generate two spaced beams in orthogonal circular polarization by variable rotation technique," *IEEE Transactions on Antennas and Propagation*, vol. 68, no. 6, pp. 4617–4626, 2020.

[35] E. Baladi, M. Y. Xu, N. Faria, J. Nicholls, and S. V. Hum, "Dual-band circularly polarized fully reconfigurable reflectarray antenna for satellite applications in the Ku-band," *IEEE Transactions on Antennas and Propagation*, vol. 69, no. 12, pp. 8387–8396, 2021.

[36] Z. Zhang, H. Luyen, J. H. Booske, and N. Behdad, "A dual-band, polarization-rotating reflectarray with independent phase control at each band," *IEEE Transactions on Antennas and Propagation*, vol. 69, no. 9, pp. 5546–5558, 2021.

[37] H. Yang, F. Yang, X. Cao, S. Xu, J. Gao, X. Chen, M. Li, and T. Li, "A 1600-element dual-frequency electronically reconfigurable reflectarray at X/Ku-band," *IEEE transactions on antennas and propagation*, vol. 65, no. 6, pp. 3024–3032, 2017.

[38] K. K. Karnati, Y. Shen, M. E. Trampler, S. Ebadi, P. F. Wahid, and X. Gong, "A bst-integrated capacitively loaded patch for Ka- and X-band beamsteerable reflectarray antennas in satellite communications," *IEEE Transactions on Antennas and Propagation*, vol. 63, no. 4, pp. 1324–1333, 2015.

[39] F. Faraz, Y. Huang, H. Liu, T. U. R. Abbasi, X. Wang, L. Si, and W. Zhu, "High-efficiency dual-band metasurface with independent multifold geometric phases," *Advanced Optical Materials*, p. 2300347, 2023.

[40] W.-L. Guo, G.-M. Wang, H.-S. Hou, K. Chen, and Y. Feng, "Multifunctional coding metasurface for dual-band independent electromagnetic wave control," *Optics Express*, vol. 27, no. 14, pp. 19 196–19 211, 2019.

[41] D. Rotshild and A. Abramovich, "Ultra-wideband reconfigurable X-band and Ku-band metasurface beam-steerable reflector for satellite communications," *Electronics*, vol. 10, no. 17, p. 2165, 2021.

[42] M.-A. Chung, K.-C. Tseng, and I.-P. Meiy, "Antennas in the internet of vehicles: Application for X band and Ku band in low-earth-orbiting satellites," *Vehicles*, vol. 5, no. 1, pp. 55–74, 2023.

[43] I.-J. Hwang, D.-J. Yun, J.-I. Park, Y.-P. Hong, and I.-H. Lee, "Design of dual-band single-layer metasurfaces for millimeter-wave 5G communication systems," *Applied Physics Letters*, vol. 119, no. 17, 2021.

[44] A. K. Fahad, R. Nazir, and C. Ruan, "Simple design of broadband polarizers using transmissive metasurfaces for dual band Ku/Ka band applications," *Sensors*, vol. 22, no. 23, p. 9152, 2022.

[45] X. Tong, Z. H. Jiang, Y. Li, F. Wu, J. Wu, R. Sauleau, and W. Hong, "An integrated dual-band dual-circularly-polarized shared-aperture transmitarray antenna for K-/Ka-band applications enabled by polarization twisting elements," *IEEE Transactions on Antennas and Propagation*, 2023.

[46] "ESA website," https://www.esa.int/Applications, accessed: 10-07-2023.

[47] M. Magarotto *et al.*, "Design of a plasma-based intelligent reflecting surface," *Physics of Plasmas*, vol. 30, no. 4, 2023.

[48] F. Sadeghikia, K. Zafari, M.-R. Dorbin, M. Himdi, and A. K. Horestani, "Reconfigurable biconcave lens antenna based on plasma technology," *Scientific Reports*, vol. 13, p. 9213, 2023.

[49] M. A. Lieberman and A. J. Lichtenberg, *Principles of plasma discharges and materials processing*. John Wiley & Sons, 2005.

[50] M.-R. Dorbin, A. K. Horestani, F. Sadeghikia, M. T. Noghani, and H. Jaafar, "Analytical study on the resonance frequency of tunable surface-wave-excited plasma antennas," *IEEE Transactions on Antennas and Propagation*, vol. 70, no. 10, pp. 9073–9082, 2022.

[51] F. Sadeghikia, M. Valipour, M. T. Noghani, H. Ja'afar, and A. K. Horestani, "3d beam steering end-fire helical antenna with beamwidth control using plasma reflectors," *IEEE Transactions on Antennas and Propagation*, vol. 69, no. 5, pp. 2507–2512, 2020.

[52] P. Nayeri, F. Yang, and A. Z. Elsherbeni, *Reflectarray antennas: theory, designs, and applications*. John Wiley & Sons, 2018.

[53] C. A. Balanis, *Antenna theory: analysis and design*. John wiley & sons, 2015.

[54] A. Daykin-Iliopoulos *et al.*, "Characterisation of a thermionic plasma source apparatus for high-density gaseous plasma antenna applications," *Plasma Sources Science and Technology*, vol. 29, no. 11, p. 115002, 2020.

[55] A. B. Petrin, "On the transmission of microwaves through plasma layer," *IEEE Transactions on Plasma Science*, vol. 28, no. 3, pp. 1000–1008, 2000.

[56] T. J. Cui, M. Q. Qi, X. Wan, J. Zhao, and Q. Cheng, "Coding metamaterials, digital metamaterials and programmable metamaterials," *Light: science & applications*, vol. 3, no. 10, pp. e218–e218, 2014.

[57] F. Costa and M. Borgese, "Electromagnetic model of reflective intelligent surfaces," *IEEE Open Journal of the Communications Society*, vol. 2, pp. 1577–1589, 2021.

[58] T. Li and Z. N. Chen, "Wideband sidelobe-level reduced Ka-band metasurface antenna array fed by substrate-integrated gap waveguide using characteristic mode analysis," *IEEE Transactions on Antennas and Propagation*, vol. 68, no. 3, pp. 1356–1365, 2019.

[59] N. Yu and F. Capasso, "Flat optics with designer metasurfaces," *Nature materials*, vol. 13, no. 2, pp. 139–150, 2014.

[60] M. Di Renzo, A. Zappone, M. Debbah, M.-S. Alouini, C. Yuen, J. De Rosny, and S. Tretyakov, "Smart radio environments empowered by reconfigurable intelligent surfaces: How it works, state of research, and the road ahead," *IEEE Journal on Selected Areas in Communications*, vol. 38, no. 11, pp. 2450–2525, 2020.

[61] E. Ozturk and B. Saka, "Multilayer minkowski reflectarray antenna with improved phase performance," *IEEE Transactions on Antennas and Propagation*, vol. 69, no. 12, pp. 8961–8966, 2021.

[62] N. M. Estakhri and A. Alu, "Wave-front transformation with gradient metasurfaces," *Physical Review X*, vol. 6, no. 4, p. 041008, 2016.

[63] M. Manente *et al.*, "Regulus: A propulsion platform to boost small satellite missions," *Acta Astronautica*, vol. 157, pp. 241–249, 2019.

[64] N. Bellomo *et al.*, "Design and in-orbit demonstration of regulus, an iodine electric propulsion system," *CEAS Space Journal*, vol. 14, no. 1, pp. 79–90, 2022.

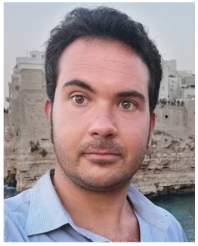

MIRKO MAGAROTTO (M'23) received an M. Sc. degree in aerospace engineering and a Ph.D. in science technology and measurements for space from the University of Padova, Padova, Italy, in 2015 and 2019, respectively. He is a Assistant Professor (RTDa) with the Dept. of Information Engineering, University of Padova. His current research interests are plasma antennas, plasma numerical simulation, and electric space propulsion.

LUCA SCHENATO (M'06) received an M.Sc. degree in telecommunication engineering and a Ph.D. in electronic and telecommunication engineering from the University of Padova, Padova, Italy, in 2003 and 2007. He is an Assistant Professor (RTDb) with the Dept. of Information Engineering, University of Padova. His research interests include optical fiber sensors, optical fiber-based devices, and intelligent reflective surfaces.

MARCO SANTAGIUSTINA (M'06) received the M.Sc. degree in electronic engineering and the Ph.D. in electronic and telecommunication engineering from the University of Padova, Padova, Italy, in 1992 and 1996, respectively. He is a Full Professor at the Dept. of Information Engineering, University of Padova. His current research interests include nonlinear optics, optical fibers, and electromagnetic field theory.

ANDREA GALTAROSSA (FM'18) is a Full Professor of Electromagnetic Waves and Photonics at the Dept. of Information Engineering, University of Padova, Italy. He has co-authored more than 200 papers in journals and conference proceedings. His research activity is mainly in optical fiber design, distributed characterization of single mode and special fibers, and distributed sensing. He has been the Topical Editor and Deputy Editor for Optics Letters. He has been a member of the Technical Program Committee for the European Conference on Optical Communication (ECOC) and the Optical Fiber Communication Conference (OFC). He is a Fellow of IEEE and OPTICA.

ANTONIO-DANIELE CAPOBIANCO (M'10) received an M.Sc. degree in electronic engineering and a Ph.D. in electronic and telecommunication engineering from the University of Padova, Padova, Italy, in 1989 and 1994, respectively. He is an Associate Professor with the Dept. of Information Engineering, University of Padova. His current research interests include theory and numerical modeling in photonics, plasmonics, and microwave antennas.